THE JOURNAL OF BIOLOGICAL CHEMISTRY VOL. 291, NO. 24, pp. 12601–12611, June 10, 2016

Two Different Functions of Connexin43 Confer Two Different Bone Phenotypes in Zebrafish*

Received for publication, February 5, 2016, and in revised form April 24, 2016 Published, JBC Papers in Press, April 25, 2016, DOI 10.1074/jbc.M116.720110

Akihiro Misu[‡], Hiroaki Yamanaka[‡], Toshihiro Aramaki[‡], Shigeru Kondo[‡§], I. Martha Skerrett[¶], M. Kathryn Iovine[‖], and Masakatsu Watanabe[‡1]

From the [‡]Graduate School of Frontier Biosciences, Osaka University, 1-3 Yamadaoka, Suita, Osaka 565-0871, Japan, [§]CREST, Japan Science and Technology Agency, 1-3 Yamadaoka, Suita, Osaka, 565-0871, Japan, the [¶]Biology Department, Buffalo State College, Buffalo, New York 14222 , and the [‖]Department of Biological Sciences, Lehigh University, Bethlehem, Pennsylvania 18015

Fish remain nearly the same shape as they grow, but there are two different modes of bone growth. Bones in the tail fin (fin ray segments) are added distally at the tips of the fins and do not elongate once produced. On the other hand, vertebrae enlarge in proportion to body growth. To elucidate how bone growth is controlled, we investigated a zebrafish mutant, *steopsel* (*stp*^{tl28d}). Vertebrae of *stp*$^{tl28d/+}$ fish look normal in larvae (~30 days) but are distinctly shorter (59–81%) than vertebrae of wild type fish in adults. In contrast, the lengths of fin rays are only slightly shorter (~95%) than those of the wild type in both larvae and adults. Positional cloning revealed that *stp* encodes Connexin43 (Cx43), a connexin that functions as a gap junction and hemichannel. Interestingly, *cx43* was also identified as the gene causing the *short-of-fin* (*sof*) phenotype, in which the fin ray segments are shorter but the vertebrae are normal. To identify the cause of this difference between the alleles, we expressed Cx43 exogenously in *Xenopus* oocytes and performed electrophysiological analysis of the mutant proteins. Gap junction coupling induced by Cx43^{stp} or Cx43^{sof} was reduced compared with Cx43-WT. On the other hand, only Cx43^{stp} induced abnormally high (50× wild type) transmembrane currents through hemichannels. Our results suggest that Cx43 plays critical and diverse roles in zebrafish bone growth.

Vertebrate bones develop during embryonic stages and grow continuously as body size increases. Because bone shape and size determine body shape, the mechanisms that generate and maintain bone shape are of great interest to biologists. Recent studies have increased our knowledge of bone formation mechanisms. Interactions among three types of cells—osteoblasts, osteocytes, and osteoclasts—play major roles in bone formation and bone remodeling (1–8).

Zebrafish (*Danio rerio*) is a model organism for developmental and genetic studies, and several mutants related to bone formation have been identified and analyzed (9–13). Mutant bone formation phenotypes can be categorized into two types: bone development mutants and bone growth mutants. Genes corresponding to bone development mutants are usually expressed at early developmental stages of bone formation (type 1), and bone malformations are detected when the bones first appear in embryo (14–16). On the other hand there are several zebrafish bone growth mutants, in which bone development looks almost normal at early stages, but mutant phenotypes appear at late stages (type 2) (17–19).

In this study, we focused on the *stoepsel* (*stp*) mutant fish (20) to study bone morphogenesis in adult stages. The *stp* mutant was originally isolated by a large scale screen of zebrafish mutants induced by ENU[2] (20). This mutant looks normal until ~35 days after fertilization (dpf); however, the vertebrae of the mutant fish become shorter than those of wild type fish at later growth stages. The *stp* allele is dominant and homozygous lethal. We re-examined the *stp* phenotypes in detail using modern techniques, and we performed positional cloning to identify the *stp* gene. Surprisingly, we isolated a mutation in the *connexin43* gene, which is known as the *sof* (*short-of-fin*) gene in zebrafish (21). *sof* is a well studied type 2 zebrafish mutant, in which fin segments are short in the caudal fin (21). Four *sof* mutant alleles were isolated by mutagenesis screening, and three single mutations that cause amino acid substitutions in Connexin43 protein were identified (22). In the *sof*^{b123} allele, no amino acid substitution was identified in the *connexin43* gene, but *cx43* expression was reduced in the mutant fish (21, 23, 24).

Connexin proteins are four-pass transmembrane proteins that are subunits of gap junctions (25). Approximately 20 connexin genes are known from the mammalian genome, and ~36 connexin genes are predicted in the zebrafish genome (26, 27). Six connexin proteins make a hexamer called a connexon; docking of two connexons on adjacent cells creates a gap junction. Gap junctions allow movement of small molecules (<1000 Da; *e.g.* ATP, inositol trisphosphate, ions, etc.) between neighboring cells; a connexon acts as a hemichannel on the cytoplasmic membrane (25). *connexin43* is one of the most studied connexin genes because it is linked to several human diseases (28–30). Oculodentodigital dysplasia is one Cx43-related human disease, which causes small eyes, underdeveloped teeth, and malformed fingers (31, 32). To identify the cause of the substan-

* This work was supported by Ministry of Education, Culture, Sports, Science, and Technology in Japan KAKENHI Grant 22127003 (to S. K.); by the Core Research for Evolutional Science and Technology (CREST), Japan Science and Technology Agency (to S. K.); and by Japanese Society for the Promotion of Science KAKENHI Grant 26291049 (to M. W.). The authors declare that they have no conflicts of interest with the contents of this article.

[1] To whom correspondence should be addressed: Graduate School of Frontier Biosciences, Osaka University, 1-3 Yamadaoka, Suita, Osaka 565-0871, Japan. Tel.: 81-6-6879-7997; Fax: 81-6-6879-7977; E-mail: watanabe-m@fbs.osaka-u.ac.jp.

[2] The abbreviations used are: ENU, *N*-ethyl-*N*-nitrosourea; AP, anterior-posterior; dpf, days after fertilization; DV, dorsoventral; TALEN, transcription activator-like effector nucleases.

TABLE 1

SNP Markers used in positional cloning

SNP Markers were developed from comparison of sequences between AB and *stp*. Locations of SNP Markers are on the Zv9 assembly. Both forward (F) and reverse (R) primers were used for sequencing. All SNPs were assessed by sequencing reads.

Location	PCR and sequencing primers	SNP		
		AB	*stp*	
20:40.54	F– TCGCTATTTCCGATTTTTGG	AAAAGAC	AAACGAC	at approximately 190bp
	R– GCTCCGCTGGATGTAGAGAC	TTGAAGA	TTGGAGA	at approximately 270bp
20:40.55	F– GTTGGTAGGTGGTCGCAGAT R– TCGGCTTCGATGACTTTCTT	TGCATTT	TGCCTTT	at approximately 438bp
20:40.75	F– GCATGAACTTGAAGGGGAAC R– CGTTTGAAGAGCACGTAGAAG	TCTGGGT	TCTTGGT	at approximately 439bp
20:41.01	F– CACCAAAACGACACAATTCG	GCGCCGC	GCGTCGC	at approximately 393bp
	R– ATCTGACACACCGTCAACCA	CTCCATG	CTCTATG	at approximately 409bp
20:41.25	F– CAGAACACTGCTGCCACATT R– AGGTCAGGTGACCCATCTTG	AATGCAC	AATACAC	at approximately 144bp

tial difference in phenotype between the *sof* and *stp* alleles of *cx43*, we performed electrophysiological experiments and found that the growth-dependent malformation of *stp* vertebrae is likely caused by aberrant hemichannel activity of Cx43^{stp} rather than reduced gap junction intercellular conductance observed in Cx43^{sof}.

Experimental Procedures

Animal Care—All experiments in this study were conducted in accordance with the guidelines and approved protocols for animal care and use (approval number FBS-14-002-1) at Osaka University (Osaka, Japan). We used the Tu and AB strains as wild type zebrafish lines. *stoepsel* (*stp*^{tl28d}) mutant was obtained from the Tubingen Zebrafish Stock Center.

Clearing and Measuring of Vertebral Length and Height—Fish samples were fixed with 3.7% formaldehyde and treated with ethanol to remove lipids. Then they were transferred back to H_2O. Next, samples were incubated in a saturated aqueous solution of sodium tetraborate for 1 day. Then they were incubated overnight in clearing solution (30% saturated aqueous solution of sodium tetraborate with 3 mg/ml trypsin) at 48 °C to clear the samples. Transparent samples were dyed with bone dye solution (90 mM KOH, 50 μg/ml alizarin red S) for 1 day and then incubated in 90 mM KOH for 1 day. Finally, samples were immersed in glycerol with thymol and preserved.

CT Scanning—A LaTheta LCT-100 (Hitachi Aloka Medical, Ltd.) x-ray micro-CT scanner at Osaka Bioscience Institute and an inspeXio SMX-100CT microfocus x-ray CT system at Shimadzu Corporation were used for taking CT images of bone structure. Fish samples were fixed with 3.7% formaldehyde and stored in PBS. Samples were scanned in air.

Positional Cloning and Sequence Analyses—The *stp*$^{tl28d/+}$ (TE background) mutant was crossed with the wild type AB strain. TE is a mixture of Tu and TL lines. Here, we used Tu instead of TE. F1 heterozygous fish were backcrossed with wild type parents, and F2 fish were used for genetic mapping. *stp* was mapped to chromosome 20 by checking simple sequence length polymorphism markers. Then *stp* was mapped between single nucleotide polymorphisms listed in Table 1, which were identified within chromosome 20 (40.55–41.01 Mb). Gene predictions were derived from Ensemble (Sanger Institute). Candidate gene sequencing was performed using a 3130 Genetic Analyzer (Applied Biosystems).

Rescue of stp Homozygote Phenotype—A *cx43* fragment was cloned from a bacterial artificial chromosome clone (DKEY-261A18) with a forward primer (5′-GCTCGAGTCTATGAA-TGGGATGAG-3′) and a reverse primer (5′-GGGCGGCCGC-TAGACGTCCAGGTCATCAG-3′) and ligated into a Tol2 plasmid (pT2AL200R150G) (33). The *cx43* sequence was injected into *stp*$^{tl28d/+}$ embryos to generate *Tg*(*cx43*pro-*cx43*)*stp*$^{tl28d/+}$ transgenic fish lines. *Tg*(*cx43*pro-*cx43*)*stp*$^{tl28d/tl28d}$ transgenic fish were made by crossing *stp*$^{tl28d/+}$ fish and *Tg*(*cx43*pro-*cx43*)*stp*$^{tl28d/+}$ fish.

cx43 Reporter Line—The *cx43* promoter sequence was cloned from a bacterial artificial chromosome clone (DKEY-261A18) with a forward primer (5′-CCGGCTCGAGGCTTA-AAGGGTCACGAAACACC-3′) and a reverse primer (5′-GGC-CGGATCCTTGAGGGAGTTCTAGCTGAAAATA-3′) and ligated into a Tol2 plasmid (pT2AL200R150G). A reporter construct of *cx43* was made by inserting mCherry cDNA downstream of the *cx43* promoter region.

TALEN-mediated cx43 Knock-out—Transcription activator-like effector nucleases (TALEN) pairs for *cx43* knock-out were designed using the TALEN Targeter program (available at the Cornell University website). TAL repeats were assembled using a Golden Gate TALEN and TAL Effector kit 2.0 (34) with some modifications (35) and cloned into expression vectors pCS2TAL3DD or pCS2TAL3RR (36). The TALEN expression plasmids were linearized by NotI digestion, and then mRNAs were *in vitro* transcribed using an mMESSAGE mMACHINE SP6 transcription kit (Ambion). Synthetic TALEN mRNAs were injected into one-cell stage embryos (100 pg/embryo each). To test the efficacy of mutagenesis, TALEN mRNA-injected embryos were harvested 1 day after fertilization. The genomic DNA was extracted, and the loci containing the TALEN target sequence were amplified by PCR with a forward primer (5′-TTCAAGTGTCACCAAAGTGTCT-3′) and a reverse primer (5′-CTGCTGGGTATTGCACTTGA-3′). TALEN-induced mutations were detected by T7 endonuclease I assay. The most effective TALEN pair was used for *cx43* knock-out. The target sequence is 5′-TCTGGCTCTCTGTG-CTCTtcatcttccggatccTTGTTCTGGGAACAGCA-3′ (TALEN binding sequences are shown in uppercase, and spacer sequence is in lowercase).

Measurement of mRNA Expression for cx43 Alleles—To precisely compare the expression levels of the wild type and mutated alleles, which differ at only one nucleotide, we generated cDNA clones from the heterozygous fish and then sequenced them. mRNAs were collected from tail fins of *stp*$^{tl28d/+}$ fish and *stp*^{tl28d}/*sof*^{b123} fish by RNeasy Protect mini kit (Qiagen), respectively. Then mRNAs were reverse-transcribed using SuperScript III reverse transcriptase (Invitrogen). The *cx43* sequence around the *stp* mutation site was amplified from the cDNAs, and the amplified fragments were cloned with plasmid vector. Then *Escherichia coli* colonies were picked up randomly, and DNA fragments in the plasmid were sequenced. The frequencies of DNA fragments derived from *stp* allele or wild type allele in *stp*$^{tl28d/+}$ fish and DNA fragments from the *stp* allele and *sof* allele in *stp*^{tl28d}/*sof*^{b123} were compared.

Preparation of Connexin mRNA and Injection into Xenopus Oocytes—Connexin cDNAs were amplified using PCR and cloned into pGEM-HeFx plasmid (37). The plasmids were linearized using restriction enzyme and then applied to the mRNA preparation kit (T7 mMessage mMachine; Ambion) according to the manufacturer's protocol. An adult *Xenopus laevis* female was anesthetized with MS-222, and the ovarian lobes were collected using a surgical knife and forceps. The eggs were treated with collagenase solution (2 mg/ml collagenase I (Sigma) and 2 mg/ml hyaluronidase (Sigma) in OR2 buffer: 82.5 mM NaCl, 2 mM KCl, 1 mM $MgCl_2$, and 5 mM HEPES, adjusted to pH 7.5 using NaOH) at 18 °C for 2 h. Stage V and VI oocytes were collected manually and used for mRNA injection. Then mRNA (0.05 ng for gap junction recording; 5 ng for hemichannel recording) was co-injected with 10 ng of antisense oligonucleotide DNA for *Xenopus cx38* into *Xenopus* oocytes. For the negative control, only antisense oligonucleotide was injected. Oocytes injected with mRNA were incubated overnight at 18 °C in 1/2× diluted L15 medium (Sigma) with 2 mM $CaCl_2$ (HEPES-buffered and adjusted to pH 7.5 with NaOH).

Voltage Clamp Recording—Vitelline membranes of mRNA-injected oocytes were removed manually using forceps in a hypertonic solution (200 mM aspartic acid, 1 mM $MgCl_2$, 10 mM EGTA, 20 mM KCl, and 10 mM HEPES, pH 7.5). The oocytes were manually paired, touching at the vegetal poles, while in ND96(+) solution (93.5 mM NaCl, 2 mM KCl, 1.8 mM $CaCl_2$, 2 mM $MgCl_2$, and 5 mM HEPES). The transjunctional current was measured using the dual whole cell voltage clamp technique. Current and voltage electrodes were prepared with a micropipette puller P-1000 (Sutter Instruments) to obtain a resistance of 0.5–1.0 MΩ. The pipette was filled with solution containing 3 M KCl, 10 mM EGTA, and 10 mM HEPES (pH 7.4). Voltage clamp experiments were performed using two Multi Electrode Clamp Amplifiers iTEV90 (HEKA). To measure the transjunctional current, both cells were initially clamped at −40 mV, and one cell was then subjected to alternating pulses of from −160 to +80 mV in 20-mV increments. Currents detected in the second oocyte were recorded, and junctional conductance was calculated using the current value at the end of each 3-s pulse (steady state). The conductance was obtained by $G_j = I_j/(V_1 - V_0)$, and normalized G_j values were compared.

Hemichannel Recording—Hemichannel currents were recorded from a single oocyte using a Multi Electrode Clamp Amplifier iTEV90. Modified ND96(+) solution with/without 2 mM $CaCl_2$ was used as a bath solution. To obtain the hemichannel current, the cells were initially clamped at −40 mV and then subjected to 5-s voltage steps from −30 to +60 mV in 10-mV increments.

Western Blotting and Immunofluorescence Staining—*Xenopus* oocytes, in which the antisense oligonucleotide for *Xenopus cx38* and mRNA for *cx43*, *cx43*^{stp}, or *cx43*^{sof} were injected, were harvested after overnight incubation. Then each oocyte was used for Western blotting and immunofluorescence staining. Western blotting was performed using anti-Cx43 antibody (Santa Cruz Biotechnology). Anti-β-tubulin antibody (Cell Signaling) was used for the positive controls. Signals were detected using ECL Western blotting detection kit (GE Healthcare). Immunofluorescence staining was performed using the anti-Cx43 antibody and Alexa 488 conjugated antibody (Invitrogen). Pictures were taken using a BZ-X700 microscope (KEYENCE) with OP-66835 BZ filter GFP.

Results

Stoepsel (stp^{tl28d}*) Phenotype*—The *stp* mutation was isolated in a large scale screen of zebrafish mutants induced by ENU (20). In the original paper, *stp* was described as a mutant associated with abnormalities of the axial skeleton (Fig. 1, *A* and *A′*). *stp* homozygous (*stp*$^{tl28d/tl28d}$) fish die from edema of the eye and abdomen at ~10 dpf (Fig. 2, *A–C*). Because wild type zebrafish start to form vertebrae along the notochord at ~14 dpf, we could not observe the bone phenotype in *stp*$^{tl28d/tl28d}$ fish. Heterozygous mutants (*stp*$^{tl28d/+}$) had similar body lengths to the wild type at early stages, but during later growth they gradually became shorter relative to the wild type along the anterior-posterior (AP) axis (Fig. 1, *A* and *A′*). The number of vertebrae appeared similar between the mutant and wild type fish. The body height along the dorsoventral (DV) axis was not affected by the *stp* mutation (Fig. 1, *B* and *B′*).

Next, we examined the bone phenotype in detail by microCT scanning (Figs. 1, *B–F* and *B′–F′*, and 3). AP length (Fig. 3*A*), DV height (Fig. 3*B*), and the proportions (Fig. 3*C*) of corresponding vertebrae (identification numbers from anterior to posterior) were compared between wild type and *stp* mutant fish. Vertebrae in *stp*$^{tl28d/+}$ fish were obviously shorter along the AP axis than those of wild type fish (Fig. 3*A*), whereas the head and fins did not differ notably (Fig. 1, *B* and *B′*).

Each vertebra is composed of a centrum and appendixes, which include a ventral arch (Fig. 1, *C*, *C′*, *D*, and *D′*, *red arrowheads*), hemal arch (Fig. 1, *C*, *C′*, *D*, and *D′*, *green arrowheads*), and complex beam structures (Fig. 1, *C* and *C′*, *blue arrowheads*). The centrum appears at ~14 dpf. The appendixes form after centrum growth. In a wild type centrum, an hourglass-like structure was seen along the AP axis (Fig. 1*E*). On the other hand, in *stp*$^{tl28d/+}$ mutants, the hourglass-like structure was distorted and sometimes filled with clots (Fig. 1, *D′* and *E′*). Although the centrum was malformed in the *stp*$^{tl28d/+}$ mutant, the hemal arch (Fig. 1, *C′* and *D′*, *green arrowheads*), neural arch (Fig. 1, *C′* and *D′*, *red arrowheads*), and beam structures (Fig. 1*C′*, *blue arrowhead*) were approximately normal. These data indicate that the *stp* mutation mainly affected the formation of the centrum of the vertebrae.

Next, to reveal when vertebral malformation occurred, we investigated the time course of centrum growth (Fig. 1, *G–I*). We measured the AP length (Fig. 1*G*) and DV height (Fig. 1*H*) of the centrums of caudal (No. 1–5) vertebrae (Fig. 3). Graphs in Fig. 1 (*G–I*) show that early vertebral development (35 dpf) was not affected by the *stp* mutation; however, after 35 dpf, centrum growth was abnormally low along the AP axis (Fig. 1*G*), but not along the DV axis (Fig. 1*H*). This suggests that the *stp* mutation affects the mechanism that maintains appropriate vertebral shape during growth.

Cloning the Gene Affected by the stp Mutation—To identify the gene affected by the *stp* mutation, we next performed positional cloning and identified a critical region of 460 kb in chromosome 20 (Fig. 4*A*). This region contains eight genes, of which

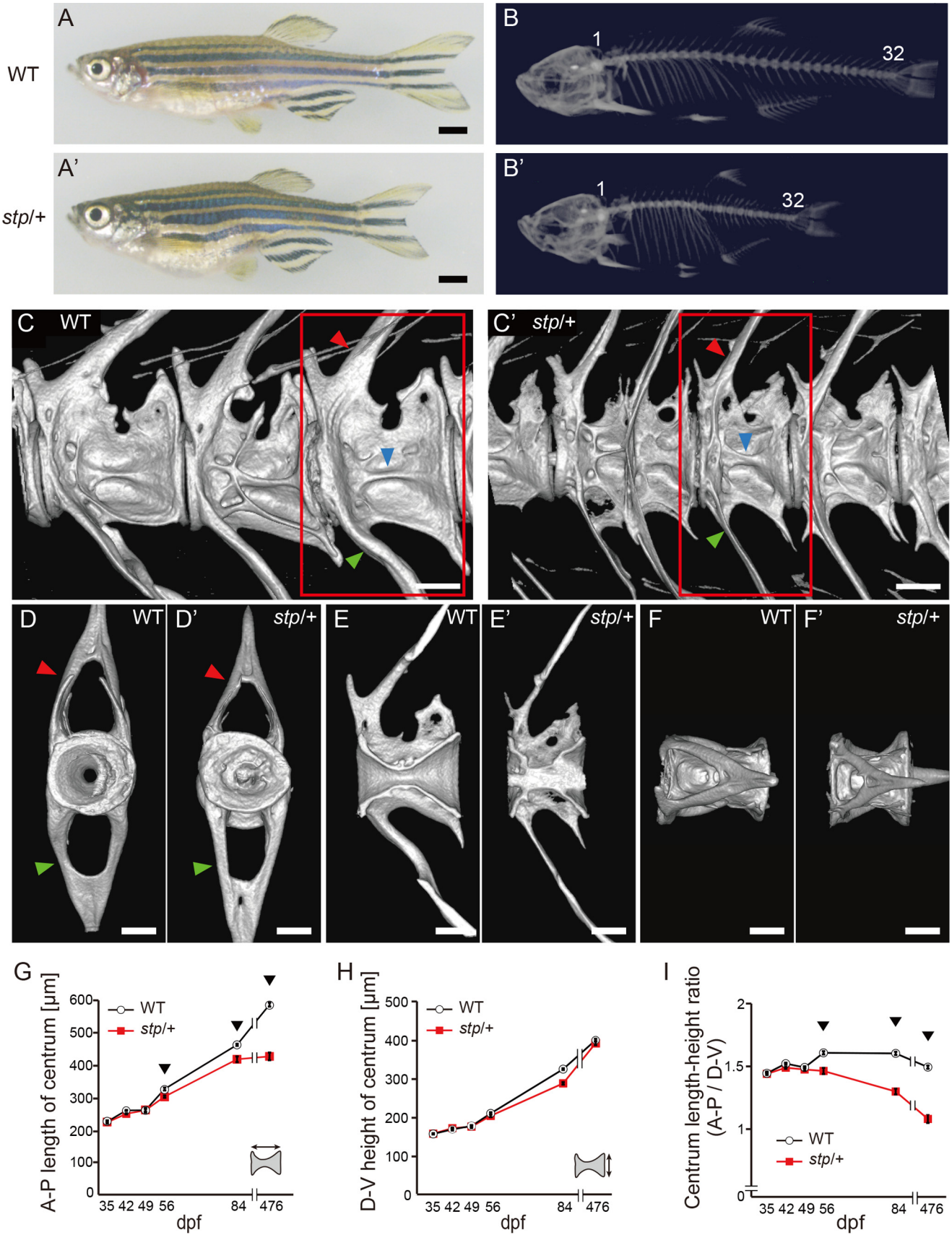
A
WT
A'
stp/+
B
1
32
B'
1
32
C WT
C' stp/+
D WT
D' stp/+
E WT
E' stp/+
F WT
F' stp/+
G
A-P length of centrum [µm]
600
500
400
300
200
100
0
WT
stp/+
35 42 49 56
84
476
dpf
H
D-V height of centrum [µm]
500
400
300
200
100
0
WT
stp/+
35 42 49 56
84
476
dpf
I
Centrum length-height ratio (A-P / D-V)
2
1.5
1
0
WT
stp/+
35 42 49 56
84
476
dpf

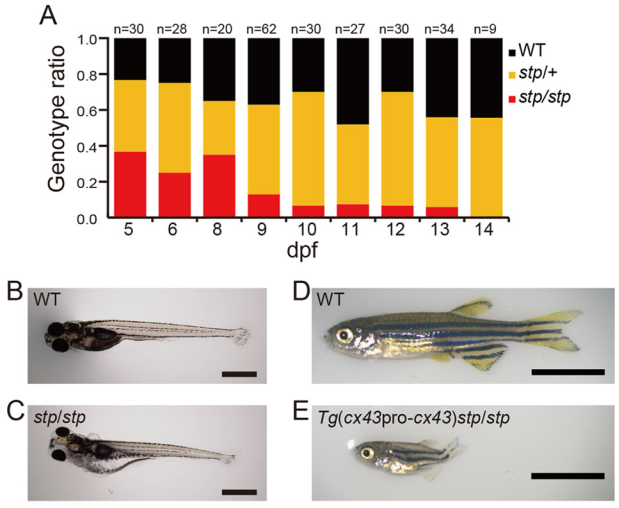

FIGURE 2. **Phenotypes of $stp^{tl28d/tl28d}$ and *Tg*(*cx43*pro-*cx43*)$stp^{tl28d/tl28d}$ fish.** *A*, genotype ratio of $stp^{tl28d/tl28d}$ and siblings at each time point. Larvae derived from crossing $stp^{tl28d/+}$ and $stp^{tl28d/+}$ were harvested at indicated day and genotyped. *B* and *C*, wild type and $stp^{tl28d/tl28d}$ larvae at 13 dpf. *D* and *E*, wild type and *Tg*(*cx43*pro-*cx43*)$stp^{tl28d/tl28d}$ fish at 56 dpf. *Scale bars*, 1000 μm in *B* and *C* and 5000 μm in *D* and *E*. *stp*/+, $stp^{tl28d/+}$; *stp*/*stp*, $stp^{tl28d/tl28d}$.

six genes code for connexins (*cx*). The coding sequences of the *stp* allele were sequenced, and their amino acid sequences were compared with the wild type. Among the eight genes, only the *cx43* gene had a point mutation (G233T) specific to the *stp* allele, which altered the amino acid sequence (tryptophan → leucine: W78L) (Fig. 4*B*). The amino acid substitution occurs in the second transmembrane domain of the Cx43 protein (Fig. 4*C*). A BLAST search revealed that the region around the mutation was highly conserved in vertebrates (Fig. 4*D*). To confirm *cx43* expression in vertebrae, we generated transgenic fish that expressed mCherry under the control of the *cx43* promoter (Fig. 4, *E*, *E′*, *F*, and *F′*). This transgenic fish showed mCherry expression at the growing edges of the centrum, where the defect resulting in the *stp* phenotype was expected to occur (Fig. 4, *E* and *E′*), and at the junctions between fin bones (Fig. 4, *F* and *F′*).

stp Gene Knock-out by TALEN—To confirm that the mutation in *cx43* is responsible for the *stp* phenotype, we knocked out the *stp* allele of *cx43* using TALEN. The TALEN construct was designed to target the middle region of the first extracellular loop of Cx43, just at the 5′ side of the *stp* mutation (Fig. 5*A*). TALEN mRNA was injected into embryos of $stp^{tl28d/+}$ fish, and we isolated the F1 fish that had a frameshift in the *stp* allele (Fig. 5*B*). Because *stp* (Fig. 5, *D* and *D′*) is a dominant mutation, knock-out of the *stp* allele in $stp^{tl28d/+}$ fish should rescue the phenotype. The heterozygous fish, which had the frameshifted *stp* allele and the wild type *cx43* allele (*KO*/+; Fig. 5, *E* and *E′*), did not show any difference in centrum structure compared with wild type siblings (Fig. 5, *C*, *C′*, and *H*), indicating that knock-out of the *stp* allele rescued vertebral structure. Vertebrae in *stp* mutants were 12% shorter than in the wild type, but vertebral lengths were similar in KO/+ fish and the wild type (Fig. 5*H*). This result confirmed that the mutation in *cx43* (Cx43W78L) is responsible for the *stp* phenotype.

We also examined the lethality of the *stp* homozygote. If the lethality was caused by the loss of normal Cx43 protein, survival of $stp^{tl28d/tl28d}$ larvae should be rescued by introducing exogenous wild type *cx43*. We generated *Tg*(*cx43*pro-*cx43*)$stp^{tl28d/tl28d}$ fish by introducing a wild type *cx43* gene. *Tg*(*cx43*pro-*cx43*)$stp^{tl28d/tl28d}$ fish did not die at larval stages and grew into adults (Fig. 2, *D* and *E*). Interestingly the rescued fish showed a unique phenotype (Fig. 2*E*): they had very short body lengths compared with the wild type fish (Fig. 2*D*) and *stp*/+ heterozygous fish (Fig. 1*A′*). These results suggest that the lethality of $stp^{tl28d/tl28d}$ results from the loss of *cx43* function. In addition this transgenic fish also suggested that Cx43W78L has a dominant negative effect on wild type Cx43 because the transgene, cx43pro-cx43, did not rescue the *stp* phenotype perfectly (Fig. 2*E*).

Another cx43 Mutant, Short Fin—The zebrafish mutant, *sof*, which exhibits short fin bone segments, also involves *cx43* (21). There are four reported *sof* alleles. All of these alleles show similar recessive phenotypes. Three alleles have amino acid substitutions in *cx43*, and one allele causes low expression of *cx43*. It is very puzzling that these alleles of the same gene do not cause shortening of vertebrae. We first examined the amount of *cx43* mRNA between *stp* and sof^{b123} (low expression allele) and found that the expression of mRNA from the *stp* allele was comparable with that from the wild type *cx43* allele (Fig. 6*A*); however, expression of mRNA from the sof^{123} allele was less than one-tenth that of the *stp* allele (Fig. 6*B*).

We then investigated the shape of sof^{b123} mutant fish to determine whether they had morphologically normal vertebrae. As shown in Fig. 5 (*F*, *F′*, and *H*), vertebrae of both $sof^{b123/b123}$ and $sof^{b123/+}$ fish are normal in size and shape. These data indicated that a simple decrease of *cx43* mRNA level did not affect vertebral growth. However, the vertebrae of *stp*/sof^{b123} fish are drastically shorter than those of $stp^{tl28d/+}$ fish (Fig. 5, *G*, *G′*, and *H*), suggesting that the wild type Cx43 protein compensates for the dominant effect of the *stp* allele. When the amount of normal Cx43 protein was decreased, the *stp* phenotype (short vertebrae) became more evident.

Next, we measured the length of fin ray segments for fish carrying the different *cx43* alleles (Fig. 5*I*) to see whether the *stp* allele causes defects in fin bones. Segment lengths of $sof^{b123/b123}$ and $sof^{b123/+}$ fish were 64 and 87% of wild type, respectively. This showed that fin ray length is sensitive to the amount of

FIGURE 1. ***stp* vertebral phenotype.** Panels show adult fish (*A* and *A′*), CT scans of their skeletons (*B*–*F* and *B′*–*F′*), and graphs of vertebral growth rate (*G*–*I*). *B* and *B′*, the *numbers* indicate vertebra identity along the AP axis. The $stp^{tl28d/+}$ fish had the same number of vertebrae as their wild type siblings ($n = 6$). *C* and *C′*, the *red square* indicates the third caudal vertebra. *Arrowheads* point to neural arches (*red arrowheads*), hemal arches (*green arrowheads*), and beam-like structures (*blue arrowheads*) on the centrums. *D* and *D′*, front views of the third vertebra. Abnormal calcification was seen in the inside of the centrum in $stp^{tl28d/+}$ fish. It was also seen in the wild type fish, but calcification was more severe in the $stp^{tl28d/+}$ fish. *E* and *E′*, sagittal images from the left side. *F* and *F′*, views from the top. *G*, centrum length at each time point. *H*, centrum DV height at each time point. *I*, centrum length to height ratio. *G*–*I*, the data shown are mean values from five vertebrae, the first through the fifth caudal vertebrae ($n = 6$). *Arrowheads* point to time points at which the *stp* vertebral phenotype was seen. *Error bars*, S.E. *Scale bars*, 1000 μm in *A* and *A′* and 250 μm in *C*–*F* and *C′*–*F′*. *stp*/+, $stp^{tl28d/+}$.

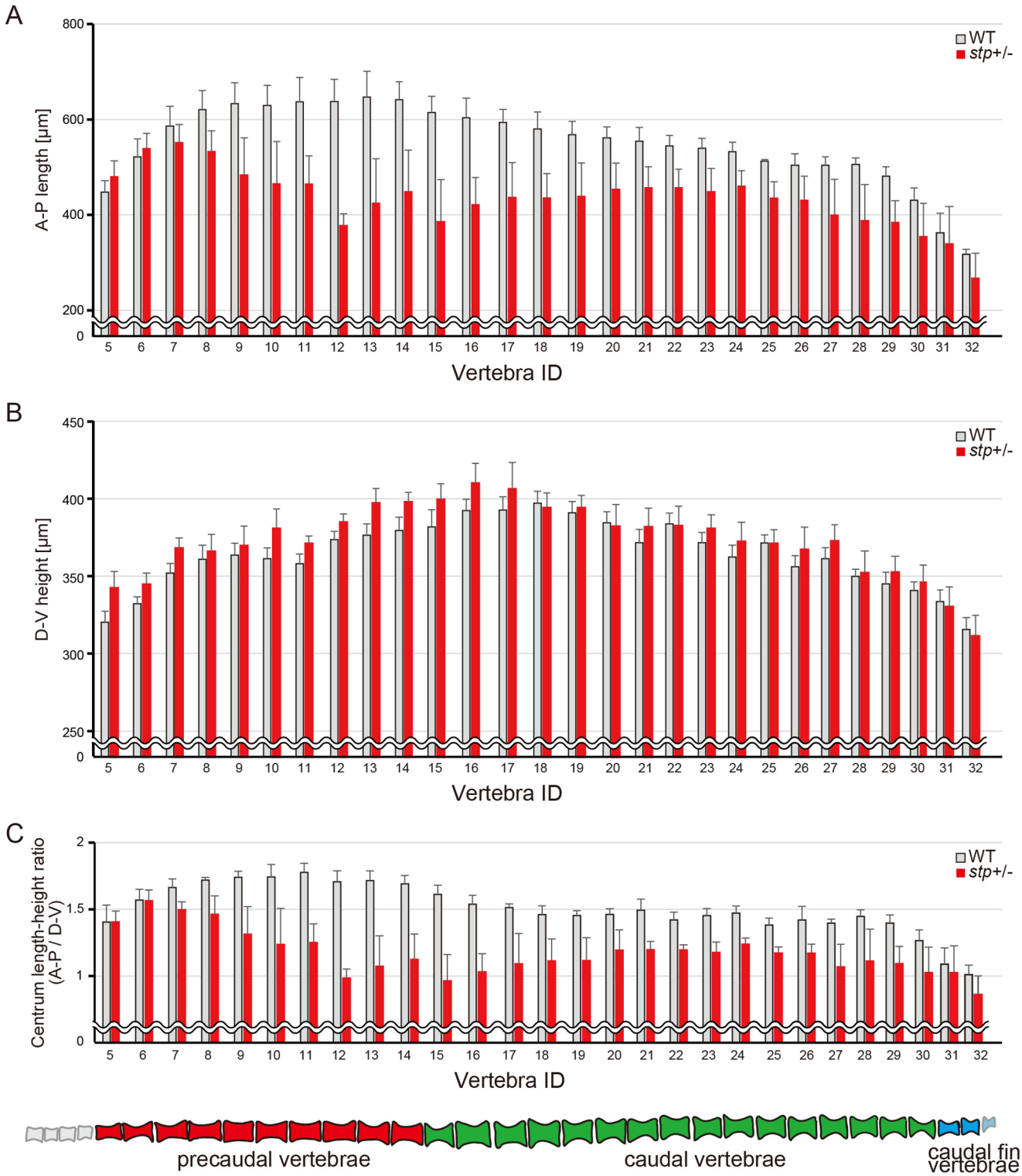

FIGURE 3. **Graphs of centrum length and height.** *A–C*, AP length (*A*), DV height (*B*), and the ratio (*C*) of centrum length/height of each vertebra at 476 dpf ($n = 6$). Six $stp^{tl28d/+}$ fish and their siblings were compared. *Error bars*, S.E. *stp*/+, $stp^{tl28d/+}$.

Cx43 protein. $stp^{tl28d/+}$ fish also had shorter fin ray segments than wild type fish, but the difference was only 5% (Fig. 5*I*, *arrowhead 1*). The difference of the fin ray segment length between *stp*/sof^{b123} and $sof^{b123/+}$ fish was 7% (Fig. 5*I*, *arrowhead 2*). Therefore, the *stp* allele also causes the short fin bone phenotype, but the severity is less than that of the *sof* alleles.

Functional Analysis of $Cx43^{stp}$—As described above, the influence of the *stp* allele is severe in vertebrae but mild in fin bones. On the other hand, the influence of the sof^{b123} allele is undetectable in vertebrae (Fig. 5*H*) and severe in fin bones. This apparent discrepancy suggests that the Cx43 protein has more than one distinct function. It is known that there are two distinct functions of connexins: formation of gap

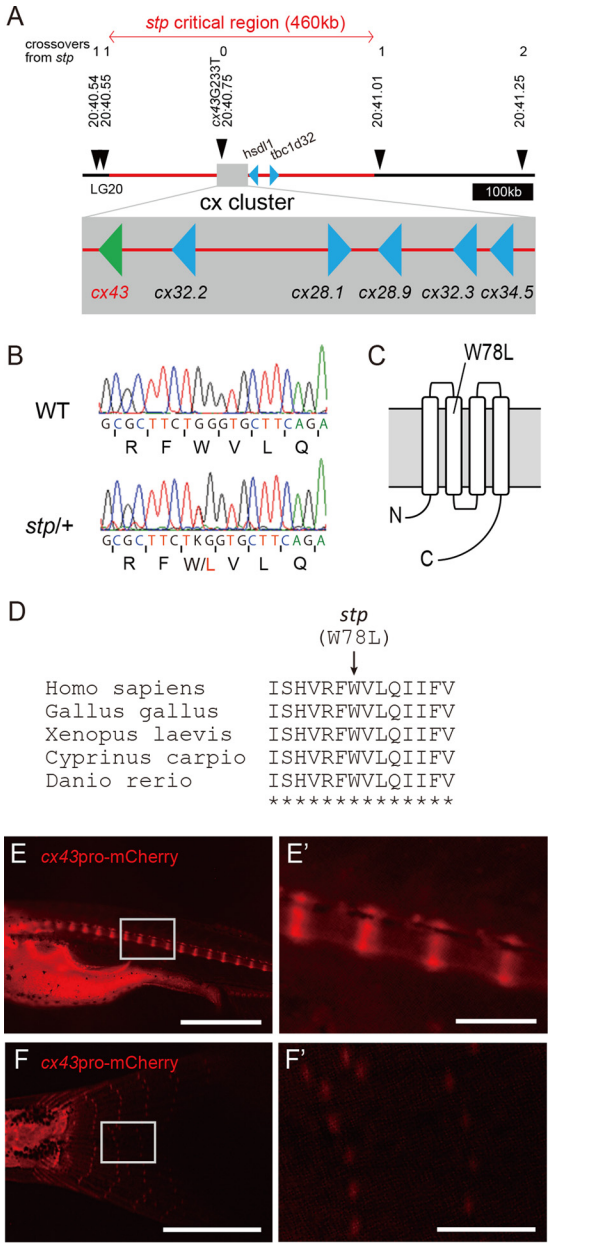

FIGURE 4. **The *stp* allele exhibits a lesion in *cx43*.** *A*, meiotic mapping of the *stp* allele revealed ~460 kb of contiguous sequence of the *stp* region. Only *cx43* exhibits an ENU-induced lesion. *Red lines* represent the region spanning the *stp* critical interval. *B*, electrophoretograms showing the mutation identified in the coding sequence of the *stp* allele. *C*, cartoon of Cx43 protein in a double-lipid bilayer indicating the location of the ENU-induced lesion. *D*, BLAST search results showing the highly conserved amino acid sequence of Cx43. *E*, *E′*, *F*, and *F′*, expression of mCherry fluorescent protein in the vertebrae and caudal fin, driven by the *cx43* promoter. *E* and *E′*, mCherry was expressed at the growing edges of vertebral centrums of 21 dpf fish. *F* and *F′*, mCherry was expressed at junctions between fin ray segments of 36 dpf fish. *Scale bars*, 1000 μm in *E* and *F* and 200 μm in *E′* and *F′*.

junctions or hemichannels. We examined both functions of Cx43^{sof} and Cx43^{stp} electrophysiologically. There are three known *sof* missense mutations: Cx43F30V, Cx43P191S, and Cx43F209I. A previous paper reported that all of them have similar hemichannel and gap junction activity (22). Here, we used *cx43*^{j7e2} (which codes for Cx43P191S) as a representative *sof* mutant.

To examine gap junction activity of these Cx43 mutants, we performed voltage clamp current recording using *Xenopus* oocytes. In this study, we injected only 0.05 ng of mRNAs for Connexin proteins into each oocyte because we detected very large transjunctional currents when we injected 5 ng of mRNA for wild type Cx43 (22). Fig. 7*A* shows examples of junctional currents induced by wild type Cx43 (Cx43-WT) and Cx43W78L (Cx43^{stp}). Cx43W78L (Cx43^{stp}) showed reduced junctional currents between the oocytes compared with Cx43-WT (Fig. 7*B*). On the other hand Cx43P191S (Cx43^{sof}) did not show significant junctional current in this experimental condition (0.05 ng of mRNA/oocyte).

We next examined the hemichannel activities of wild type and mutant Cx43s. *Panels A* and *B* of Fig. 8 show current traces of Cx43-WT and Cx43W78L (Cx43^{stp}), and *panels C–G* summarizes the current-voltage relationship of these hemichannels. As reported previously, Cx43-WT and Cx43P191S (Cx43^{sof}) did not increase current in comparison with the negative control (Fig. 8, *C*, *E*, and *G*). On the other hand Cx43W78L (Cx43^{stp}) induced extraordinarily high hemichannel activity (Fig. 8*D*), which was more than 50-fold greater than that of Cx43-WT. We examined the hemichannel activity of Cx43W78L (Cx43^{stp}) co-expressed with Cx43-WT, mimicking the situation in *stp*$^{tl28d/+}$ fish *in vivo*. The hemichannel activity of Cx43W78L (Cx43^{stp}) co-expressed with Cx43-WT was also very high (Fig. 8*F*). Assuming that wild type and mutant connexins interact heteromerically, these results suggest that heteromeric hemichannels of Cx43-WT and Cx43W78L (Cx43^{stp}) in *stp*$^{tl28d/+}$ fish would have increased activity. These results suggest that the hemichannel activity of Cx43P191S (Cx43^{sof}) is similar to that of Cx43-WT, whereas that of Cx43W78L (Cx43^{stp}) is abnormally increased.

To determine the protein expression and functional changes of connexin proteins in *Xenopus* oocytes, we performed Western blotting and immunofluorescence staining. The *bracket* in Fig. 9*A* indicated that Cx43 and its mutants were expressed in *Xenopus* oocyte, although several bands were detected in the Cx43W78L (Cx43^{stp}) lane. The bands detected in Cx43W78L imply that the W78L mutation causes a protein modification defect in Cx43. Further study is needed to determine whether this modification of Cx43 is related to the *stp* phenotype. 50-kDa bands in Fig. 9*A* are due to nonspecific binding of the anti-Cx43 antibody used in this study. The *arrow* in Fig. 9*A′* indicates the expression of β-tubulin (positive control). Protein localization of Cx43 and its mutants were also examined, and membrane localization was detected by immunofluorescence staining (Fig. 9, *B*—*E* and *B′*–*E′*). Compared with the wild type Cx43 (Fig. 9*B*), the signals of Cx43W78L (Cx43^{stp}) (Fig. 9*D*) and Cx43P191S (Cx43^{sof}) (Fig. 9*E*) detected at the cell membranes looked weak (22). For the negative controls (NC), only antisense oligonucleotide for *Xenopus cx38* was injected into *Xenopus* oocytes (Fig. 9, *A*, *A′*, and *C*).

Discussion

In this paper we analyzed a zebrafish mutation that disrupts normal vertebra formation. Homozygous (*stp*$^{tl28d/tl28d}$) fish die; heterozygous (*stp*$^{tl28d/+}$) fish grow to adults but show a specific phenotype of shorter vertebrae along only the AP axis. Because

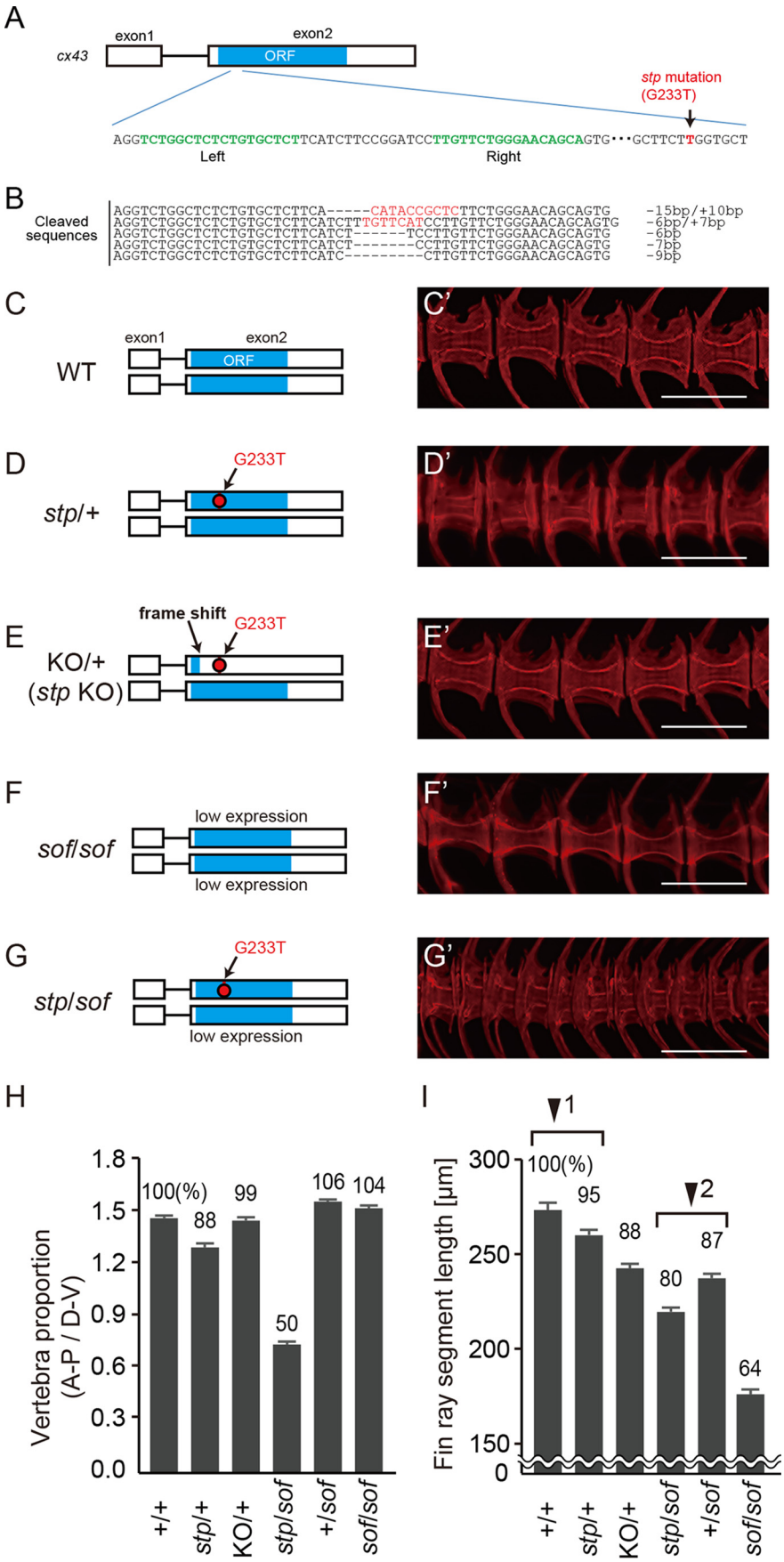
A
exon1
exon2
cx43
ORF
stp mutation
(G233T)
AGGTCTGGCTCTCTGTGCTCTTCATCTTCCGGATCCTTGTTCTGGGAACAGCAGTG···GCTTCTTGGTGCT
Left
Right
B
Cleaved sequences
AGGTCTGGCTCTCTGTGCTCTTCA-----CATACCGCTCTTCTGGGAACAGCAGTG -15bp/+10bp
AGGTCTGGCTCTCTGTGCTCTTCATCTTTGTTCATCCTTGTTCTGGGAACAGCAGTG -6bp/+7bp
AGGTCTGGCTCTCTGTGCTCTTCATCT------TCCTTGTTCTGGGAACAGCAGTG -6bp
AGGTCTGGCTCTCTGTGCTCTTCATCT-------CCTTGTTCTGGGAACAGCAGTG -7bp
AGGTCTGGCTCTCTGTGCTCTTCATC---------CTTGTTCTGGGAACAGCAGTG -9bp
C
WT
C'
D
stp/+
G233T
D'
E
KO/+
(stp KO)
frame shift
G233T
E'
F
sof/sof
low expression
low expression
F'
G
stp/sof
G233T
low expression
G'
H
Vertebra proportion (A-P / D-V)
1.8
1.5
1.2
0.9
0.6
0.3
0.0
100(%)
88
99
50
106
104
+/+
stp/+
KO/+
stp/sof
+/sof
sof/sof
I
Fin ray segment length [µm]
300
250
200
150
0
1
2
100(%)
95
88
80
87
64
+/+
stp/+
KO/+
stp/sof
+/sof
sof/sof

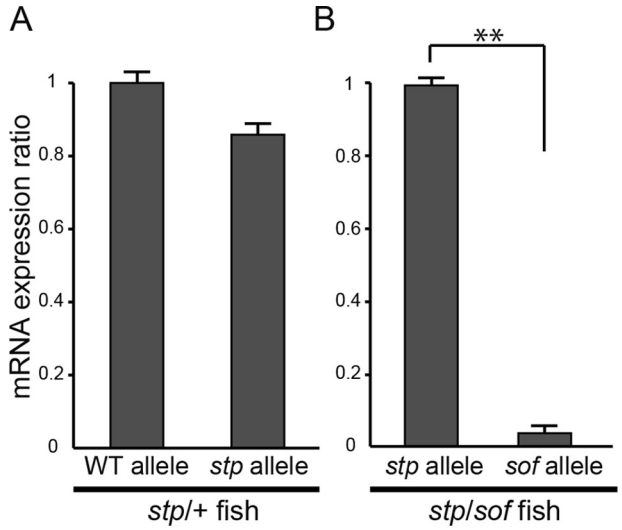

FIGURE 6. ***cx43* mRNA expression ratios in mutant fish.** *A*, *cx43* mRNA expression ratio in $stp^{tl28d/+}$ fish, normalized to WT fish. 39–48 colonies were sequenced for each fish ($n = 6$). *B*, *cx43* mRNA expression ratio in stp/sof^{b123} fish, normalized to *stp* fish. 28–48 colonies were sequenced for each fish ($n = 5$). *Error bars*, S.E. **, $p < 0.01$. *stp*/+ = $stp^{tl28d/+}$; *stp/sof* = stp/sof^{b123}.

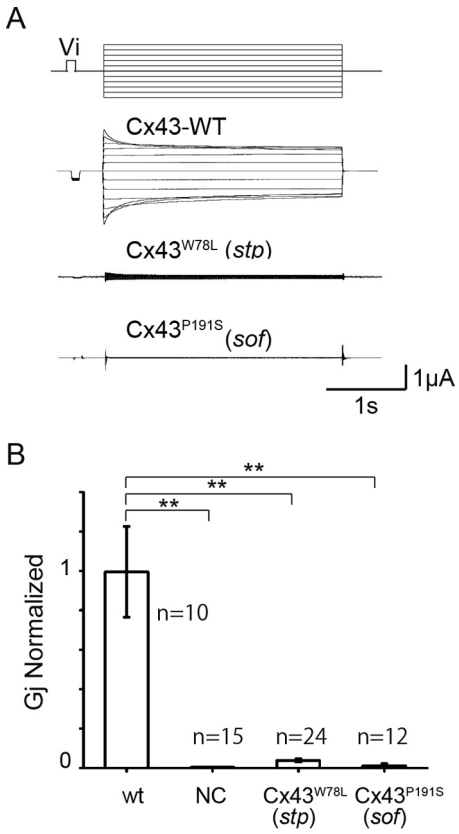

FIGURE 7. **Electrophysiological analysis of Cx43 gap junctions.** *A*, examples of junctional current traces for Cx43 (Cx43-WT), Cx43W78L ($Cx43^{stp}$), and Cx43P191S ($Cx43^{sof}$) shown below voltage protocol (*top*). *B*, normalized junctional conductance of mutants compared with Cx43-WT. *NC*, negative control (only antisense oligonucleotide for *Xenopus cx38* was injected). *Error bars*, S.E. **, $p < 0.01$.

this phenotype is not seen in young fish (~35 dpf) and becomes evident only after ~60 dpf, we deduced that the mutation caused some defect in the control of bone growth. To identify the gene altered in the *stp* mutant, we performed positional cloning and TALEN knock-out of the genomic sequence and found that a single base mutation in *cx43* causes the phenotype.

Curiously, a previous paper reported that another mutation in *cx43* is responsible for the *sof* phenotype, in which fins are short but vertebrae are normal. To determine why these alleles of the same gene differed in their effects, we investigated two different functions of connexins: as gap junctions and hemichannels. Both $Cx43^{stp}$ and $Cx43^{sof}$ showed reduced gap junction currents relative to wild type, which confirmed that the *sof* phenotype was caused by the defect in gap junction activity, as suggested by Hoptak-Solga *et al.* (22). On the other hand, $Cx43^{stp}$ hemichannels showed abnormally high (50-fold higher than wild type) conductance, whereas $Cx43^{sof}$ hemichannel conductance was almost the same as Cx43-WT. These results are consistent with the hypothesis that extremely high hemichannel activity causes the vertebral phenotype of the *stp* allele.

Although the mechanism by which gap junctions and hemichannels affect different bones is unknown, we assume that it is related to the difference in the bone forming process between vertebrae and fin bones. Fins are mechanically supported by fin rays arrayed in parallel. Each fin ray is composed of short segments of bone called lepidotrichia. Each segment is almost the same size along the AP axis (for tail fins). When the fin grows, a new fin ray segment is made at the tip of each fin ray. The newly made segments are nearly as long as the old segments along the AP axis and do not grow longer with time or with increasing fin length. On the other hand, vertebrae initially appear at ~14 days post fertilization and continuously enlarge during the growth of the fish. Therefore, we infer that Cx43 gap junctions are involved in initial bone formation, and Cx43 hemichannels are involved in later bone growth.

One proposed mechanism of mechanical stress sensing by osteocytes is as follows. When bones are exposed to mechanical stress, they deform slightly, causing movement of the fluid surrounding the osteocytes. This movement of fluid causes shear stress that induces effusion of prostaglandin E_2 through hemichannels (38). Prostaglandin E_2 promotes osteoclast differentiation by down-regulating Osteoprotegerin (39), a protein that blocks RANKL-RANK interaction and promotes osteoclast differentiation.

FIGURE 5. **Vertebral and fin ray segment phenotypes of zebrafish mutants.** *A* and *B*, knock out of $cx43^{stp}$ by TALEN. *A*, schematic of *cx43* gene structure. The *green letters* are the DNA binding sites by TALEN. The *red letter* is the *stp* mutation (G233T). *B*, Mutated sequences produced by TALEN. Three F1 lines had frame-shifting mutations, which were (−15 bp/+10 bp), (−6 bp/+7 bp), and (−7 bp). The (−15 bp/+10 bp) line was used for the *stp* gene knock-out investigation. *C–G*, vertebral structure of wild type (*C*), *stp*/+ (*D*), KO/+ (*stp* allele knock-out) (*E*), $sof^{b123/b123}$ (*F*), and stp/sof^{b123} (*G*) fish. Cleared, alizarin red S-stained specimens were made from 70 dpf fishes. KO/+ fish had a wild type allele and a knock-out *stp* allele. $sof^{b123/b123}$ fish showed normal vertebra structure, but stp/sof^{b123} fish had markedly shorter vertebrae. *H* and *I*, six mutant fish were randomly chosen and compared with six of their wild type siblings at 70 dpf. *H*, length to height ratio of vertebral centrums. *I*, length of fin ray segment. The segments second from the tail bud were measured, and average length was calculated. *Arrowheads 1* and *2* indicate pairs of fish genotypes that differ in the presence or absence of the *stp* allele. *Error bars*, S.E. *Scale bars*, 500 μm in *C′–G′*. *stp*/+, $stp^{tl28d/+}$; *sof/sof*, $sof^{b123/b123}$; *stp/sof*, stp/sof^{b123}.

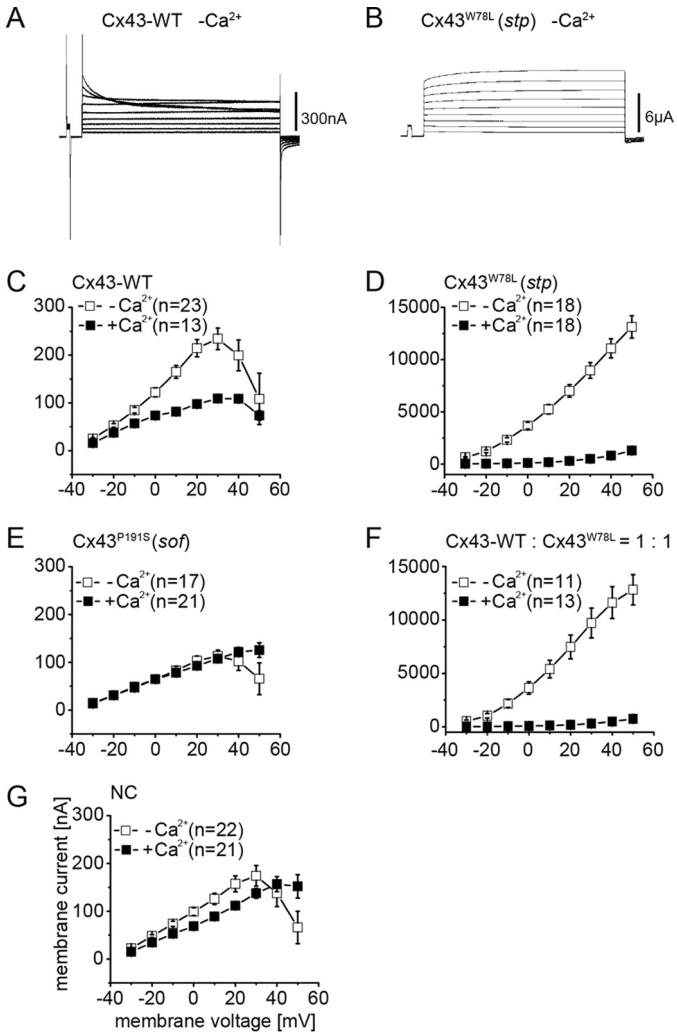

FIGURE 8. **Non-junctional current recording.** *A* and *B*, examples of hemichannel current traces for Cx43-WT (*A*) and Cx43W78L (Cx43^{stp}) (*B*). *C–G*, plots of current *versus* membrane voltage in single oocytes expressing Cx43-WT (*C*), Cx43W78L (Cx43^{stp}) (*D*), Cx43P191S (Cx43^{sof}) (*E*), Cx43-WT and Cx43W78L (Cx43^{stp}) (*F*), and negative control (only antisense oligonucleotide for *Xenopus cx38* was injected) (*G*). Oocytes voltage was pulsed from −30 to +60 mV in 10-mV steps in the presence (■) or absence (□) of 2 mM Ca^{+2} ion. *Error bars*, S.E. *NC*, negative control.

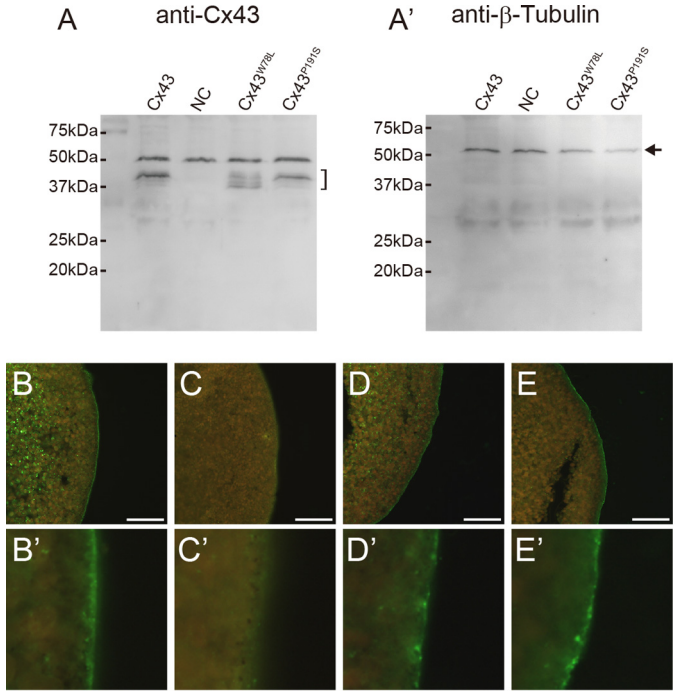

FIGURE 9. **Protein expression.** Protein expression and membrane localization in *Xenopus* oocytes were analyzed by Western blotting (*A* and *A′*) and immunofluorescence staining (*B–E* and *B′–E′*). *A*, *bracket* indicates Cx43 bands detected by anti-Cx43 antibody. Bands at ~50 kDa are nonspecific labeling. *A′*, *arrow* indicates β-tubulin bands (positive control). mRNA for each connexin was injected into *Xenopus* oocytes along with an antisense oligonucleotide for *Xenopus cx38*. *NC*, negative control (only antisense oligonucleotide for *Xenopus cx38* was injected). *B–E*, membrane localization of Cx43 or its mutants was detected. *B*, wild type Cx43. *C*, negative control. *D*, Cx43W78L (Cx43^{stp}). *E*, Cx43P191S (Cx43^{sof}). *B′–E′*, magnified images of *B–E*, respectively. *Scale bars*, 50 μm.

We hypothesize that the *stp* allele reduces vertebral elongation by mimicking high mechanical stress. We found that *cx43* expression in zebrafish vertebrae is highest in the growing edges (Fig. 4, *E* and *E′*). Because these parts of the vertebra contact the adjacent vertebra, we expect that mechanical stress is highest there. Therefore, one possible explanation for the effect of the *stp* mutation on vertebral shape is that it enhances hemichannel activity, allowing more prostaglandin E_2 effusion. This would mimic the effects of high mechanical stress and lead to increased osteoclast differentiation and, hence, increased rates of bone breakdown at the edges of the centrum.

The major finding of our study is that there are two distinct functions of Cx43 in bone formation, one of which affects early development only and one of which affects subsequent growth only. These two functions correlate with differences in the electrophysiological properties of gap junctions and hemichannels among *cx43* alleles. We hypothesize that the differences in gap junction and hemichannel function among alleles cause their differing effects on bone development and growth. Future studies are needed to test this hypothesis *in vivo*.

Author Contributions—A. M., H. Y., S. K., and M. W. designed the experimental strategy. A. M. performed positional cloning experiments. A. M. and T. A. performed transgenic experiments. A. M., H. Y., S. K., and M. K. I analyzed bone development. M. W. and I. M. S. performed electrophysiological experiments and analyzed data. A. M. prepared the manuscript, and all authors commented on the manuscript.

Acknowledgments—We thank the Shimadzu Corporation and the Osaka Bioscience Institute for lending CT scanners. We also thank H. Shirota and C. Sato at Osaka University for technical assistance in the positional cloning experiment, and Dr. T. W. White at SUNY Stony Brook for technical advice on the oocyte clamp experiments.

References

1. Attanasio, C., Nord, A. S., Zhu, Y., Blow, M. J., Li, Z., Liberton, D. K., Morrison, H., Plajzer-Frick, I., Holt, A., Hosseini, R., Phouanenavong, S., Akiyama, J. A., Shoukry, M., Afzal, V., Rubin, E. M., *et al.* (2013) Fine tuning of craniofacial morphology by distant-acting enhancers. *Science* **342,** 1241006
2. Gluhak-Heinrich, J., Ye, L., Bonewald, L. F., Feng, J. Q., MacDougall, M., Harris, S. E., and Pavlin, D. (2003) Mechanical loading stimulates dentin matrix protein 1 (DMP1) expression in osteocytes *in vivo*. *J. Bone Miner. Res.* **18,** 807–817

3. Schoenebeck, J. J., Hutchinson, S. A., Byers, A., Beale, H. C., Carrington, B., Faden, D. L., Rimbault, M., Decker, B., Kidd, J. M., Sood, R., Boyko, A. R., Fondon, J. W., 3rd, Wayne, R. K., Bustamante, C. D., Ciruna, B., *et al.* (2012) Variation of BMP3 contributes to dog breed skull diversity. *PLoS Genet.* **8,** e1002849
4. Bonewald, L. F. (2011) The amazing osteocyte. *J. Bone Miner. Res.* **26,** 229–238
5. Caetano-Lopes, J., Canhão, H., and Fonseca, J. E. (2007) Osteoblasts and bone formation. *Acta Reumatol. Port.* **32,** 103–110
6. Duplomb, L., Dagouassat, M., Jourdon, P., and Heymann, D. (2007) Concise review: embryonic stem cells: a new tool to study osteoblast and osteoclast differentiation. *Stem Cells* **25,** 544–552
7. Harada, S., and Rodan, G. A. (2003) Control of osteoblast function and regulation of bone mass. *Nature* **423,** 349–355
8. Komori, T. (2006) Regulation of osteoblast differentiation by transcription factors. *J. Cell. Biochem.* **99,** 1233–1239
9. Haffter, P., Granato, M., Brand, M., Mullins, M. C., Hammerschmidt, M., Kane, D. A., Odenthal, J., van Eeden, F. J., Jiang, Y. J., Heisenberg, C. P., Kelsh, R. N., Furutani-Seiki, M., Vogelsang, E., Beuchle, D., Schach, U., *et al.* (1996) The identification of genes with unique and essential functions in the development of the zebrafish, *Danio rerio*. *Development* **123,** 1–36
10. Kimmel, C. B., Miller, C. T., and Moens, C. B. (2001) Specification and morphogenesis of the zebrafish larval head skeleton. *Dev. Biol.* **233,** 239–257
11. Neuhauss, S. C., Solnica-Krezel, L., Schier, A. F., Zwartkruis, F., Stemple, D. L., Malicki, J., Abdelilah, S., Stainier, D. Y., and Driever, W. (1996) Mutations affecting craniofacial development in zebrafish. *Development* **123,** 357–367
12. Piotrowski, T., Schilling, T. F., Brand, M., Jiang, Y. J., Heisenberg, C. P., Beuchle, D., Grandel, H., van Eeden, F. J., Furutani-Seiki, M., Granato, M., Haffter, P., Hammerschmidt, M., Kane, D. A., Kelsh, R. N., Mullins, M. C., *et al.* (1996) Jaw and branchial arch mutants in zebrafish II: anterior arches and cartilage differentiation. *Development* **123,** 345–356
13. Schilling, T. F., Walker, C., and Kimmel, C. B. (1996) The chinless mutation and neural crest cell interactions in zebrafish jaw development. *Development* **122,** 1417–1426
14. Clément, A., Wiweger, M., von der Hardt, S., Rusch, M. A., Selleck, S. B., Chien, C. B., and Roehl, H. H. (2008) Regulation of zebrafish skeletogenesis by ext2/dackel and papst1/pinscher. *PLoS Genet.* **4,** e1000136
15. Cooper, K. L., Oh, S., Sung, Y., Dasari, R. R., Kirschner, M. W., and Tabin, C. J. (2013) Multiple phases of chondrocyte enlargement underlie differences in skeletal proportions. *Nature* **495,** 375–378
16. Gray, R. S., Wilm, T. P., Smith, J., Bagnat, M., Dale, R. M., Topczewski, J., Johnson, S. L., and Solnica-Krezel, L. (2014) Loss of col8a1a function during zebrafish embryogenesis results in congenital vertebral malformations. *Dev. Biol.* **386,** 72–85
17. Huycke, T. R., Eames, B. F., and Kimmel, C. B. (2012) Hedgehog-dependent proliferation drives modular growth during morphogenesis of a dermal bone. *Development* **139,** 2371–2380
18. Perathoner, S., Daane, J. M., Henrion, U., Seebohm, G., Higdon, C. W., Johnson, S. L., Nüsslein-Volhard, C., and Harris, M. P. (2014) Bioelectric signaling regulates size in zebrafish fins. *PLoS Genet.* **10,** e1004080
19. Iovine, M. K., and Johnson, S. L. (2000) Genetic analysis of isometric growth control mechanisms in the zebrafish caudal Fin. *Genetics* **155,** 1321–1329
20. Haffter, P., Odenthal, J., Mullins, M. C., Lin, S., Farrell, M. J., Vogelsang, E., Haas, F., Brand, M., van Eeden, F. J., Furutani-Seiki, M., Granato, M., Hammerschmidt, M., Heisenberg, C. P., Jiang, Y. J., Kane, D. A., *et al.* (1996) Mutations affecting pigmentation and shape of the adult zebrafish. *Dev. Genes Evol.* **206,** 260–276
21. Iovine, M. K., Higgins, E. P., Hindes, A., Coblitz, B., and Johnson, S. L. (2005) Mutations in connexin43 (GJA1) perturb bone growth in zebrafish fins. *Dev. Biol.* **278,** 208–219
22. Hoptak-Solga, A. D., Klein, K. A., DeRosa, A. M., White, T. W., and Iovine, M. K. (2007) Zebrafish short fin mutations in connexin43 lead to aberrant gap junctional intercellular communication. *FEBS Lett.* **581,** 3297–3302
23. Sims, K., Jr., Eble, D. M., and Iovine, M. K. (2009) Connexin43 regulates joint location in zebrafish fins. *Dev. Biol.* **327,** 410–418
24. Hoptak-Solga, A. D., Nielsen, S., Jain, I., Thummel, R., Hyde, D. R., and Iovine, M. K. (2008) Connexin43 (GJA1) is required in the population of dividing cells during fin regeneration. *Dev. Biol.* **317,** 541–548
25. Kumar, N. M., and Gilula, N. B. (1996) The gap junction communication channel. *Cell* **84,** 381–388
26. Abascal, F., and Zardoya, R. (2013) Evolutionary analyses of gap junction protein families. *Biochim. Biophys. Acta* **1828,** 4–14
27. Eastman, S. D., Chen, T. H., Falk, M. M., Mendelson, T. C., and Iovine, M. K. (2006) Phylogenetic analysis of three complete gap junction gene families reveals lineage-specific duplications and highly supported gene classes. *Genomics* **87,** 265–274
28. Becker, D. L., Phillips, A. R., Duft, B. J., Kim, Y., and Green, C. R. (2016) Translating connexin biology into therapeutics. *Semin. Cell Dev. Biol.* **50,** 49–58
29. Merrifield, P. A., and Laird, D. W. (2016) Connexins in skeletal muscle development and disease. *Semin. Cell Dev. Biol.* **50,** 67–73
30. Bai, D. (2016) Structural analysis of key gap junction domains-Lessons from genome data and disease-linked mutants. *Semin. Cell Dev. Biol.* **50,** 74–82
31. Laird, D. W. (2014) Syndromic and non-syndromic disease-linked Cx43 mutations. *FEBS Lett.* **588,** 1339–1348
32. Pizzuti, A., Flex, E., Mingarelli, R., Salpietro, C., Zelante, L., and Dallapiccola, B. (2004) A homozygous GJA1 gene mutation causes a Hallermann-Streiff/ODDD spectrum phenotype. *Hum. Mutat.* **23,** 286
33. Urasaki, A., Morvan, G., and Kawakami, K. (2006) Functional dissection of the Tol2 transposable element identified the minimal cis-sequence and a highly repetitive sequence in the subterminal region essential for transposition. *Genetics* **174,** 639–649
34. Cermak, T., Doyle, E. L., Christian, M., Wang, L., Zhang, Y., Schmidt, C., Baller, J. A., Somia, N. V., Bogdanove, A. J., and Voytas, D. F. (2011) Efficient design and assembly of custom TALEN and other TAL effector-based constructs for DNA targeting. *Nucleic Acids Res.* **39,** e82
35. Sakuma, T., Hosoi, S., Woltjen, K., Suzuki, K., Kashiwagi, K., Wada, H., Ochiai, H., Miyamoto, T., Kawai, N., Sasakura, Y., Matsuura, S., Okada, Y., Kawahara, A., Hayashi, S., and Yamamoto, T. (2013) Efficient TALEN construction and evaluation methods for human cell and animal applications. *Genes Cells* **18,** 315–326
36. Dahlem, T. J., Hoshijima, K., Jurynec, M. J., Gunther, D., Starker, C. G., Locke, A. S., Weis, A. M., Voytas, D. F., and Grunwald, D. J. (2012) Simple methods for generating and detecting locus-specific mutations induced with TALENs in the zebrafish genome. *PLoS Genet.* **8,** e1002861
37. Furutani, K., Ohno, Y., Inanobe, A., Hibino, H., and Kurachi, Y. (2009) Mutational and in silico analyses for antidepressant block of astroglial inward-rectifier Kir4.1 channel. *Mol. Pharmacol.* **75,** 1287–1295
38. Cherian, P. P., Siller-Jackson, A. J., Gu, S., Wang, X., Bonewald, L. F., Sprague, E., and Jiang, J. X. (2005) Mechanical strain opens connexin 43 hemichannels in osteocytes: a novel mechanism for the release of prostaglandin. *Mol. Biol. Cell* **16,** 3100–3106
39. Suda, K., Udagawa, N., Sato, N., Takami, M., Itoh, K., Woo, J. T., Takahashi, N., and Nagai, K. (2004) Suppression of osteoprotegerin expression by prostaglandin E2 is crucially involved in lipopolysaccharide-induced osteoclast formation. *J. immunol.* **172,** 2504–2510